

Identification and validation of CRLF1 and NRG1 as immune-related signatures in hypertrophic scar

Boya Yu^{a,b,1}, Yalei Cao^{c,1}, Shiyi Li^{a,b}, Ruiqi Bai^{a,b}, Guiwen Zhou^a, Qiang Fu^a, Liming Liang^a, Weijie Gu^{d,**}, Lixia Zhang^{a,b,*}, Minliang Chen^{a,*}

^a Department of Plastic and Reconstructive Surgery, The Fourth Medical Center of Chinese PLA General Hospital, Beijing 100048, China

^b Chinese PLA Medical School, Beijing 100853, China

^c Department of Urology, Peking University Third Hospital, Beijing 100191, China

^d Department of Dermatology, Air Force Medical Center, Air Force Medical University, Beijing 100142, China

ARTICLE INFO

Keywords:

Hypertrophic scar
WGCNA
Immune infiltration
Characteristic genes

ABSTRACT

Background: Hypertrophic scar (HTS) is a prevalent chronic inflammatory skin disorder characterized by abnormal proliferation and extracellular matrix deposition and the precise mechanisms underlying HTS remain elusive. This study aimed to identify and validate potential immune-related genes associated with hypertrophic scar formation.

Methods: Skin samples from normal ($n = 12$) and hypertrophic scar tissues ($n = 12$) were subjected to RNA-seq analysis. Differentially expressed genes (DEGs) and significant modular genes in Weighted gene Co-expression Network Analysis (WGCNA) were identified. Subsequently, functional enrichment analysis was performed on the intersecting genes. Additionally, eight immune-related genes were matched from the ImmPort database. Validation of NRG1 and CRLF1 was carried out using an external cohort (GSE136906). Furthermore, the association between these two genes and immune cells was assessed by Spearman correlation analysis. Finally, RNA was extracted from normal and hypertrophic scar samples, and RT-qPCR, Immunohistochemistry staining and Western Blot were employed to validate the expression of characteristic genes.

Results: A total of 940 DEGs were identified between HTS and normal samples, and 288 key module genes were uncovered via WGCNA. Enrichment analysis in key module revealed involvement in many immune-related pathways, such as Th17 cell differentiation, antigen processing and presentation and B cell receptor signaling pathway. The eight immune-related genes (IFI30, NR2F2, NRG1, ESM1, NFATC2, CRLF1, COLEC12 and IL6) were identified by matching from the ImmPort database. Notably, we observed that activated mast cell positively correlated with CRLF1 expression, while CD8 T cells exhibited a positive correlation with NRG1. The expression of NRG1 and CRLF1 was further validated in clinical samples.

Conclusion: In this study, two key immune-related genes (CRLF1 and NRG1) were identified as characteristic genes associated with HTS. These findings provide valuable insights into the immune-related mechanisms underlying hypertrophic scar formation.

1. Introduction

Hypertrophic scar (HTS) has been identified as one of the significant unmet challenges to global health, severely affecting the individual's quality of life [1,2]. This condition is characterized by the excessive proliferation and deposition of extracellular matrix following trauma,

which primarily influenced by genetic factors, wound conditions, and individual immunity [3,4]. HTS not only causes persistent itching and daily basis scar pain but can also lead to various complications, including scar contracture deformity, ulceration, and even canceration [5,6]. Moreover, the treatment outcomes for HTS often fall short of expectations, and the precise mechanisms driving HTS formation are not

* Correspondence to: Lixia Zhang, Minliang Chen, Department of Plastic and Reconstructive Surgery, The Fourth Medical Center of Chinese PLA General Hospital, Beijing 100048, China.

** Correspondence to: Weijie Gu, Department of Dermatology, Air Force Medical Center, Air Force Medical University, Beijing 100142, China.

E-mail addresses: guweijie113@163.com (W. Gu), vivian-0506@163.com (L. Zhang), chenml@sohu.com (M. Chen).

¹ These authors contributed equally to this study.

yet fully elucidated [7]. Hence, further investigation is needed to unravel the biological mechanisms and molecular characteristics underlying the progression of HTS.

Inflammation is a defensive response of the human body to various damaging stimuli. Immune cells play a crucial role in understanding the pathogenesis of various diseases including HTS and keloid [8,9]. Macrophages promote the transformation of fibroblasts into myofibroblasts during the epithelialization after trauma [10]. Interleukins-4 (IL-4) and IL-13 secreted by Th2 cells were reported to promote collagen synthesis and metabolism, leading to the deposition of reticular fibrin [11]. Additionally, the number and activation status of mast cells have been observed to correlate positively with the degree of scar hyperplasia [12]. Recently, the role of immune related genes in HTS has attracted attention. Through analysis of the GEO database and validation in a rabbit model, FOXF2, CCL2, and PLXDC2 have been identified as potential key genes in HTS [13]. There is an urgent need to explore the critical signatures related to the progression of HTS.

In the present study, we demonstrated differentially expressed genes (DEGs) between HTS and normal skin samples by using RNA-seq analysis. Furthermore, we combined weighted gene co-expression network analysis (WGCNA), ImmPort database and external dataset (GSE136906) to screen two characteristic genes (CRLF1 and NRG1) for identifying HTS. Finally, we verified that CRLF1 and NRG1 could serve as key molecular features involved in HTS in clinical samples. (The flowchart of the research was shown as Fig. 1).

2. Materials and methods

2.1. Collection of tissues samples

This study was approved by the Medical and Ethics Committees of the Fourth Medical Center of Chinese PLA General Hospital (2023KY140-KS001), and each patient signed an informed consent before enrolling in this study. HTS ($n = 12$) and normal ($n = 12$) skin tissues were obtained during plastic surgery. The characteristics of the patients were shown in Table S1. The skin tissues were washed twice in PBS to remove blood. Then the samples were stored in -80°C until use.

2.2. Transcriptome profiling

RNA-seq analysis was performed in skin tissues from HTS and Con group. Total RNA was extracted using Trizol reagent (thermofisher,

15,596,018) following the manufacturer's procedure. After total RNA was extracted, mRNA was purified from total RNA ($5\mu\text{g}$) using Dynabeads Oligo (dT) (Thermo Fisher, CA, USA) with two rounds of purification. The cDNA samples were sequenced using the Agilent Bioanalyzer 2100 system (Agilent Technologies, CA, USA). We performed the 2×150 bp paired-end sequencing (PE150) on an Illumina Novaseq™ 6000 (LC-Bio Technology CO., Ltd., Hangzhou, China) following the vendor's recommended protocol.

2.3. Differentially expressed genes (DEGs) analysis

The DEGs between Con and HTS were analyzed by DESeq2 software. The genes with the parameter of false discovery rate (FDR) below 0.05 and $|\log_2 \text{fold change}| \geq 1$ were considered differentially expressed genes. The DEGs were visualized by the volcano and heat plots. Furthermore, the DEGs were subjected to enrichment analysis of GO functions and KEGG pathways.

2.4. Functional enrichment analysis and pathway enrichment analysis

The gene ontology (GO) and Kyoto Encyclopedia of Genes and Genomes (KEGG) pathway enrichment analysis were performed to recognize the main biological functions and identify significantly enriched metabolic pathways or signal transduction pathways [14,15]. The GO analysis involved three components: biological process (BP), cellular component (CC), and molecular function (MF). To further filter the enriched items, the adjusted p -values was set to 0.05.

2.5. Weighted gene co-expression network analysis (WGCNA)

WGCNA was performed to explore the interactions among the genes and to establish potential modules associated with HTS. The correlation adjacency matrix was constructed and outliers were eliminated by the "WGCNA" package. Then, the "pickSoftThreshold" function was used to calculate the adjacency from the soft threshold power β and to convert it into a topological overlap matrix. We employed hierarchical cluster analysis and dynamic tree-cutting algorithm to identify modules, and assessed gene significance (GS) and module membership (MM) of the modules. The Molecular Complex Detection (MCODE) plugin of Cytoscape was used to calculate K-core value of each gene. The intersections of genes in significant module of WGCNA with DEGs were considered common genes (CGs).

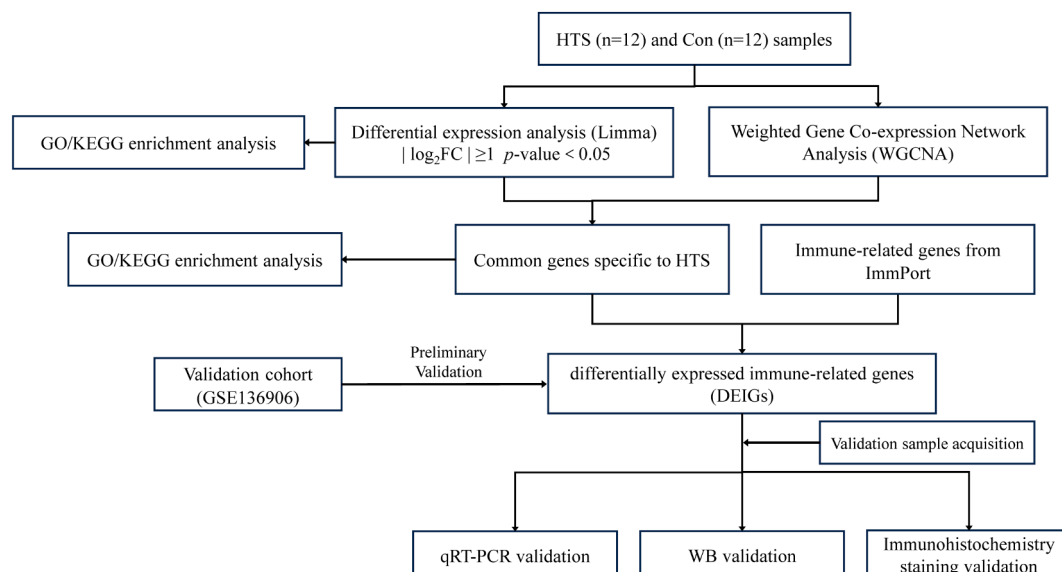


Fig. 1. The flowchart of the present study.

2.6. Association between key genes and infiltrating immune cells

Raw data of the gene expression was converted to TPM (transcripts per million) and extracted for deconvolution. The CIBERSORTx was employed for immune cell infiltration analysis. The LM22 dataset on this public platform was used as a signature matrix, which contains 547 immune cell signature genes that allow the identification of 22 human immune cells in the microenvironment [16]. Spearman correlation analysis was used to examine the correlation between the hub gene expression and immune cell abundance. The R package “ggplot2” visualized the above results.

2.7. Immunofluorescence staining

The paraffin sections were dewaxed and subjected to antigen retrieval, followed by blocking with 3% BSA for 1 h. Primary antibodies were incubated at 4 °C overnight which includes rabbit polyclonal to NRG1 (1:100, 10,527–1-AP, Proteintech, China); rabbit polyclonal to CRLF1 (1:100, YN0187, ImmunoWay Biotechnology, Plano, TX, USA); mouse monoclonal to mast cell tryptase (1:500, GB12110, Servicebio, China) and mouse monoclonal to CD8 alpha (1:1000, GB12068, Servicebio, China), respectively. Subsequently, they were washed three times with PBS and then incubated with secondary antibody for 1 h at room temperature. Nuclei were counterstained with DAPI (100 ng/mL) for 10 min at room temperature and then washed with PBS. Images were taken with a confocal microscope (Zeiss LSM880, Carl Zeiss Microscopy GmbH, Jena, Germany) at excitation wavelengths of 488 nm (green), 555 nm (red) and 405 nm (blue).

2.8. RNA isolation, reverse transcription, and real-time RT-PCR

Total RNA samples were extracted from skin tissues in HTS and Con group using Trizol reagent (thermofisher, 15,596,018) according to the manufacturer's instructions. Complementary DNA (cDNA) was synthesized using High-Capacity cDNA Reverse Transcription Kit (Applied Biosystems, USA). Real-time PCR was performed with PowerUp™ SYBR™ Green Master Mix (Applied Biosystems, CA, USA) and an QuantStudio 3 Real-Time PCR System instrument (Thermo Scientific, CA, USA). Briefly, 20 µL PCR reaction that including 1 µL of complementary DNA, 10 µL of PowerUp™ SYBR™ Green Master Mix, and 0.2 µM of each primer was used and adjusted to the final volume with double distilled H₂O (ddH₂O). While Gapdh in parallel for each run was used as an internal control. The reactions were set up on the basis of the manufacturer's protocol. PCR conditions were incubation at 50 °C for 2 min and 95 °C for 2 min followed by 40 cycles of thermal cycling (15 s at 95 °C and 1 min at 60 °C). The relative expression ratio of mRNA was quantified via the 2^(-ΔΔC_t) method. The Real-time RT-PCR primers are listed in Table 1.

2.9. Immunohistochemistry staining

The skin tissues were collected fixed in 4% paraformaldehyde fix solution for 24 h. Following dehydration through an ethanol series, the fixed skin tissues were embedded in paraffin and then sectioned. Paraffin sections (5-µm-thick) were then deparaffinized, rehydrated,

Table 1
PCR primer sequences for human.

Gene (human)	Primer	Sequence
<i>Nrg1</i>	Forward (5'-3')	TGTCACCCAGACTCCTAGCC
	Reverse (5'-3')	ACGATTACAGAGTGGCTTTCG
<i>Crlf1</i>	Forward (5'-3')	GGGATCTGGAGTGAGTGAGC
	Reverse (5'-3')	GGGTCTTGTGCGACTTCTGC
<i>Gapdh</i>	Forward (5'-3')	ACAGTCAGCCGATCTTCTT
	Reverse (5'-3')	GTTAAAGCAGCCCTGGTGA

antigen retrieved, incubated by dilution of NRG1 (1:100, 10,527–1-AP, Proteintech, China) and CRLF1 antibody (1:100, YN0187, ImmunoWay Biotechnology, Plano, TX, USA) and secondary antibody, colored by DAB colour reagent, counterstained by haematoxylin, differentiated by hydrochloric acid alcohol. Finally, the sections were dehydrated in an alcohol series and cleared in Xylene. Histological analysis was performed using digital panoramic scanner (WS-10, WISLEAP, Zhiyue Medical Technology Co., LTD; Jiangsu, China).

2.10. Western blotting

Total protein was extracted from skin tissues in ice-cold RIPA lysis buffer (Beyotime) containing 1 mM phenylmethanesulfonyl fluoride (PMSF). The homogenates were centrifuged at 12,000g for 10 min at 4 °C to yield the total protein extract in the supernatant, and then analyzed by Western blotting according. The concentration of protein was measured with a bicinchoninic acid (BCA) assay kit (Pierce/Thermo Scientific), and an equal amount of protein samples (40 µg for skin tissues) was denatured and then separated through SDS-PAGE using 10% separating gels and transferred to a PVDF membrane (Bio-Rad, Hercules, CA). The membranes were blocked with 5% nonfat milk in TBST buffer (B1009, Applygen, Applygen Technologies Inc. Beijing, China) for 60 min at room temperature and then incubated with the following primary antibodies at 4 °C overnight: rabbit polyclonal to NRG1 (1:1000, 10,527–1-AP, Proteintech, China); rabbit polyclonal to CRLF1 (1:1000, YN0187, ImmunoWay Biotechnology, Plano, TX, USA); and mouse monoclonal to GAPDH (1:3000, HC301–01, TransGen Biotech, China), respectively. The blots were incubated in horseradish peroxidase-conjugated secondary antibody including goat anti-rabbit IgG antibody (1:5000, BF03008, Biodragon Immunotechnologies, Suzhou, Jiangsu, China) or goat anti-mouse IgG antibody (1:5000, BF03001, Biodragon Immunotechnologies). Protein bands were visualized using an enhanced chemiluminescence detection kit (Pierce) followed by using a Tanon 5200 chemiluminescence detection system (Tanon, Shanghai, China). The bands were quantified with a computer-assisted imaging analysis system (Image J, NIH).

2.11. Statistical analysis

All analysis was carried out by R software (version 4.2.3), and the data from different groups were compared by Wilcoxon test. Two-tailed unpaired Student's *t*-test was used for the comparison of the mean values between two groups. All data were expressed as means ± SEM, and differences with *p* < 0.05 were considered statistically significant. The significant differences between groups were represented as * *P* < 0.05, ** *P* < 0.01.

3. Results

3.1. Identification of DEGs between HTS and con

First, we detected a total of 940 DEGs between HTS and Con samples, including 378 upregulated and 562 downregulated genes. The volcano map (Fig. 2A), the histogram (Fig. 2B) and heat plots (Fig. 2C) of DEGs were displayed. Functional enrichment analysis was carried out to clarify the underlying biological functions and pathways of DEGs. The KEGG analysis suggested that PI3K-Akt signaling pathway, Rap1 signaling pathway, cAMP signaling pathway and MAPK signaling pathway were enriched in these DEGs (Fig. 2D). The GO analysis indicated that the DEGs were predominantly enriched in multicellular organism development, signal transduction, regulation of transcription by RNA polymerase II and regulation of transcription, DNA-templated; membrane, plasma membrane, cytoplasm and integral component of membrane for CC; protein binding, metal ion binding, DNA binding and transcription factor activity, RNA polymerase II- specific hydrolase activity for MF (Fig. 2E).

3.2. WGCNA and identification of key module genes

To seek out synergistically expressed genes associated with HTS, we conducted a WGCNA to identify the key module genes in HTS. Firstly, a visible outlier was deleted by sample clustering (Fig. S1A). Next, the soft-thresholding power $\beta = 5$ (scale-free $R^2 = 0.85$) was chosen to construct a scale-free network (Fig. S1B). Then, we performed a cluster dendrogram and a dynamic tree-cutting (Fig. S1C). Subsequently, seventeen modules were identified in WGCNA that included genes with similar co-expression profiles. The salmon module exhibited the highest positive correlation with HTS compared to the other modules ($r = 0.86$; $p = 7E-8$, Fig. S1D). Therefore, the salmon module, which contains 288 genes, was considered as an HTS-associated module. We also performed co-expression network by WGCNA. The most important genes were constructed by the edge degree and k-score (Fig. S1E). Correlation analysis indicated the robust positive correlation between MM and GS in this module ($cor = 0.78$, $p = 1.4e-60$, Fig. 3A). To further investigate the function enrichment of the 288 genes, a functional enrichment analysis was performed. The GO analysis was shown in Fig. 3B. The KEGG

analysis (Fig. 3C) indicated enrichment for cellular senescence, human cytomegalovirus infection, and many immune-related pathway, such as Th17 cell differentiation, Antigen processing and presentation, Human immunodeficiency virus 1 infection and B cell receptor signaling pathway.

3.3. Selection and enrichment analysis of the CGs

We discovered 83 common genes by intersecting the genes in the salmon module with DEGs (Fig. 4A). Then we conducted enrichment analysis of CGs to find the underlying biological functions and pathways of HTS-related genes. The KEGG enrichment analysis showed enrichment for Phenylpropanoid biosynthesis, Stilbenoid, diarylheptanoid and gingerol biosynthesis, Fatty acid elongation, Nicotinate and nicotinamide metabolism, Flavonoid biosynthesis and Limonene and pinene degradation (Fig. 4B). The GO analysis suggested that the CGs were enriched in oxidation–reduction process, metabolic process, regulation of transcription, DNA – templated, protein phosphorylation and lipid metabolic process for BP; nucleus, membrane, nucleosome, integral

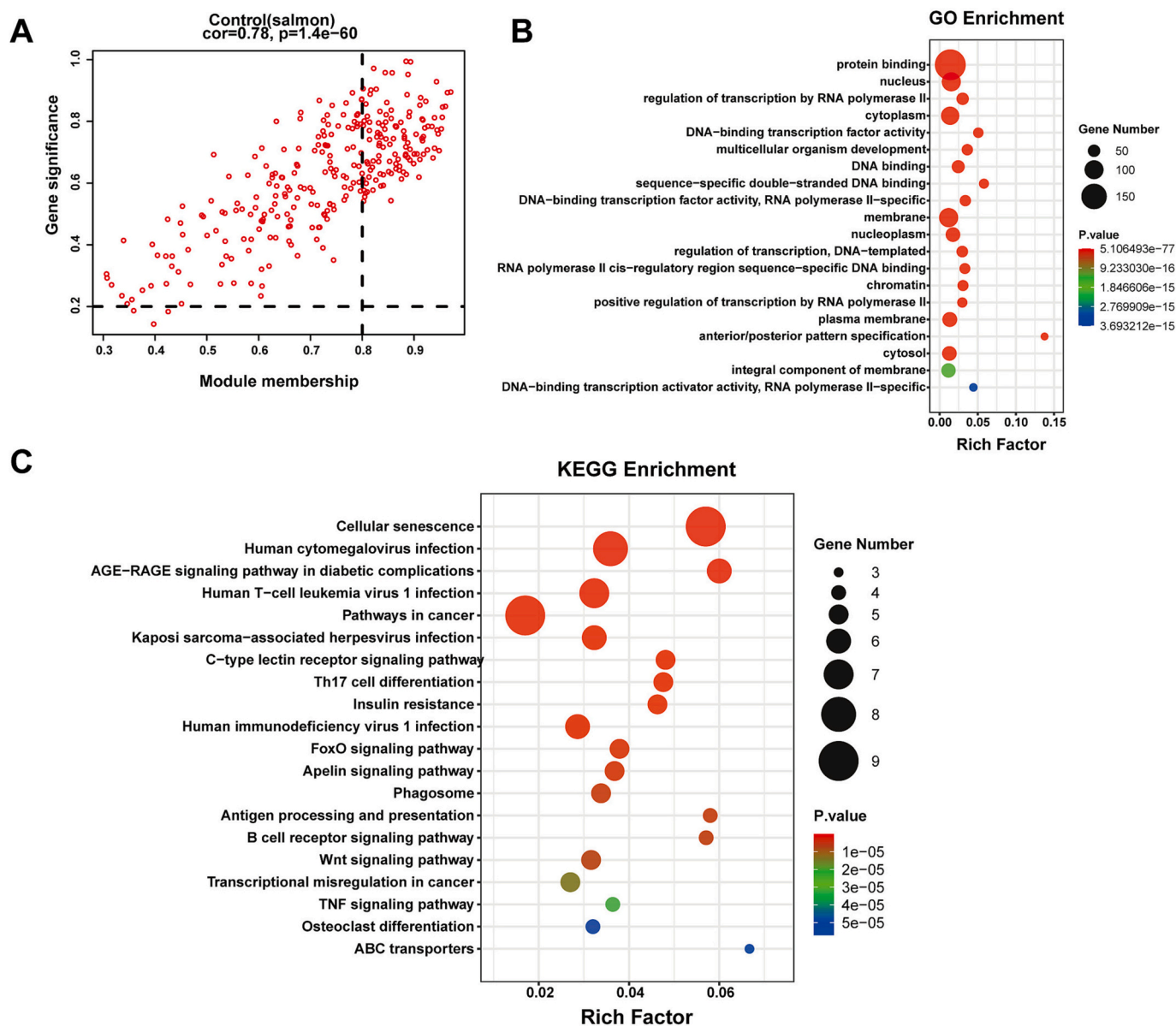


Fig. 3. The correlation and enrichment analyses of genes in salmon module. (A) A strong correlation between module membership (X-axis) and gene significance (Y-axis). (B) GO enrichment analysis of genes in salmon module. (C) The terms of KEGG enrichment analysis in salmon module.

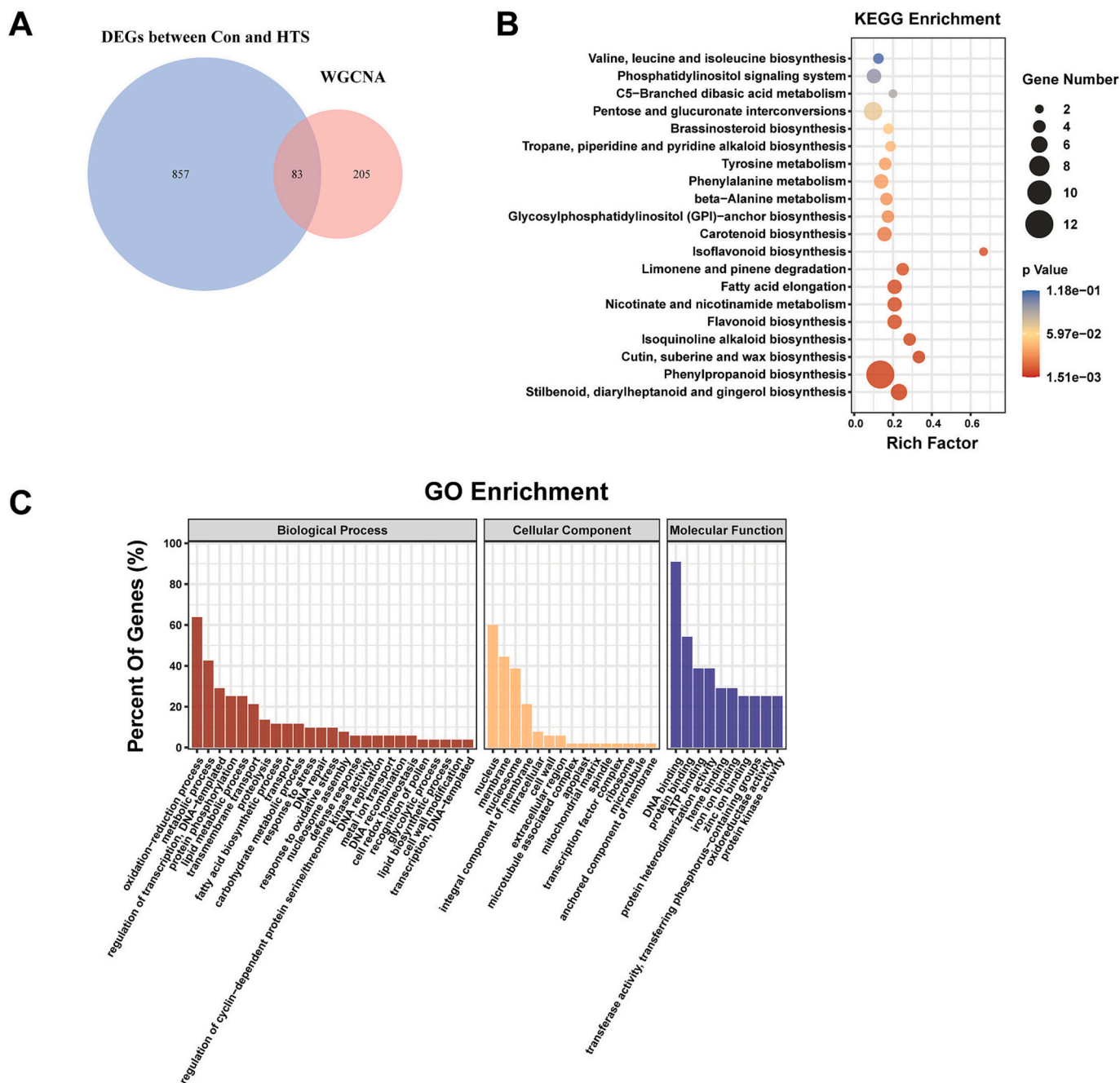


Fig. 4. (A) Venn diagram indicating the common genes between DEGs and salmon module genes. (B) KEGG enrichment analysis of the common genes. (C) GO enrichment analysis related to the common genes.

component of membrane and intracellular for CC; DNA binding, protein binding, ATP binding, protein heterodimerization activity and heme binding for MF (Fig. 4C).

3.4. Clinical validation of immune-related key genes in HTS

A total of 1793 immune-related genes were obtained from ImmPort, and eight differentially expressed immune-related genes (DEIGs) (IFI30, NR2F2, NRG1, ESM1, NFATC2, CRLF1, COLEC12, IL6) were selected by crossing CGs and 1793 immune-related genes (Fig. 5A). Then, we found only CRLF1 and NRG1 exhibited significant difference in the training cohort (GSE136906) at RNA level (Fig. 5B-C). To investigate the potential association between key genes and immune cells, we performed Spearman correlation analysis to explore the correlation between

CRLF1, NRG1 and immune cells. We discovered that immune cells with positive correlation with CRLF1 expression was activated mast cell (Fig. 5D). Meanwhile, CD8 T cells was positively correlated with NRG1 in HTS (Fig. 5D). Immunofluorescence staining revealed the number of Mast cell tryptase⁺ (mast cell marker) and CD8⁺ (CD8 T cell marker) cells were increased in HTS group with positive correlation with increased CRLF1⁺ and NRG1⁺ cells respectively (Fig. 5E). The mRNA expression of characteristic genes in 4 normal samples and 4 HTS tissues were detected. As shown in Fig. 5F-G, the expression of CRLF1 and NRG1 was significantly elevated in HTS group. Through immunohistochemistry staining, we found that the expression of CRLF1 and NRG1 was higher in the HTS samples (Fig. 5H). CRLF1 and NRG1 were mainly expressed in nucleus of fibroblasts in HTS. Moreover, at protein level, the expression of CRLF1 and NRG1 was also increased in HTS samples

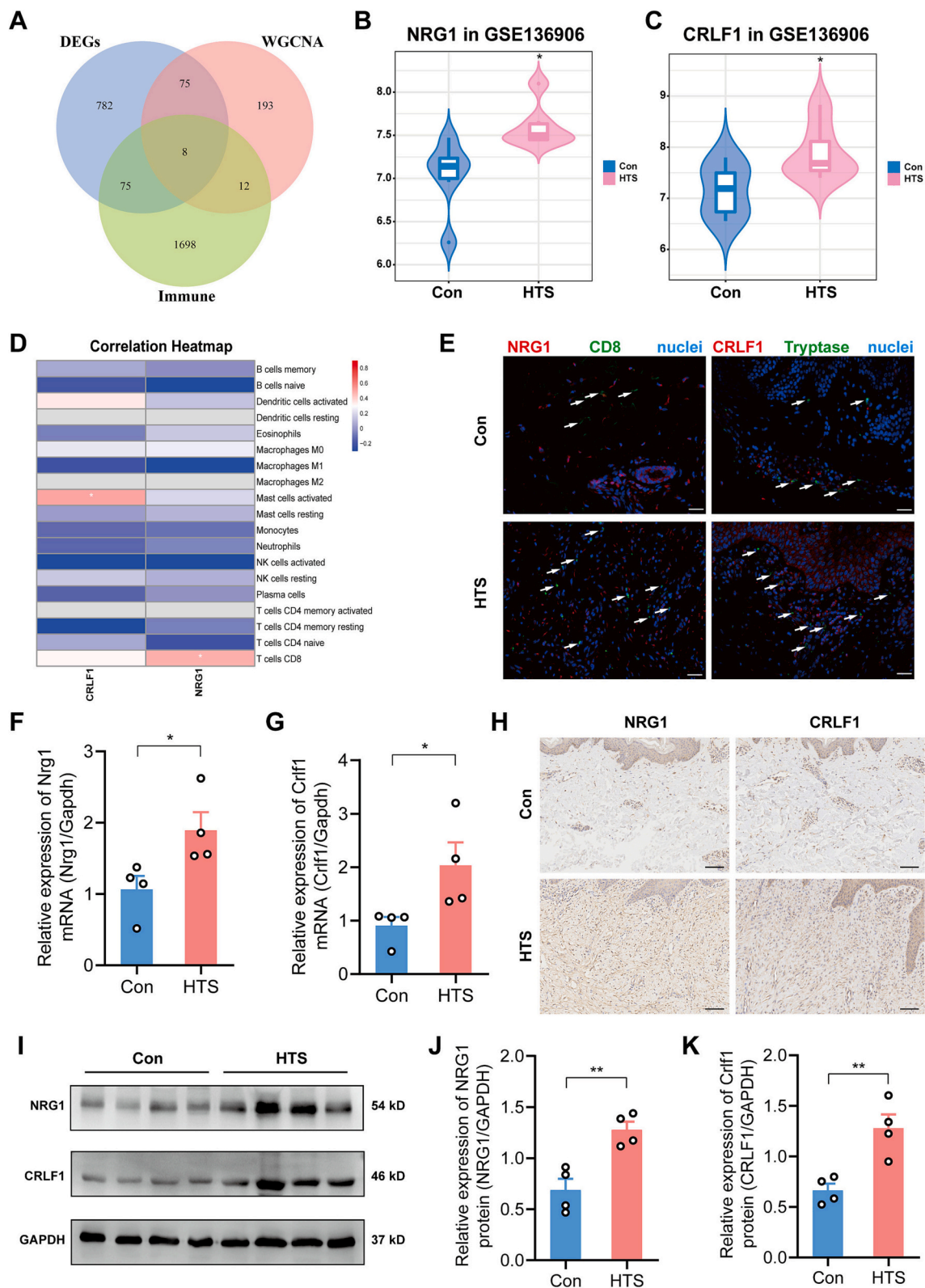


Fig. 5. Identification and verification of the expression of NRG1 and CRLF1 as potential key genes. (A) Intersection of differentially expressed genes and immune-related genes. (B–C) The violin plot demonstrates the expression of Nrg1 and Crlf1 in RNA level in GSE136906. (D) Correlation between CRLF1, NRG1 and infiltrating immune cells. Red indicates positively correlation and blue indicates negatively correlation. (E) Representative images of immunofluorescence staining in Con and HTS groups. NRG1, CRLF1, Mast cell tryptase (mast cell marker) and CD8 (CD8 T cell marker) were stained. White arrows indicate the mast cells or CD8 T cells. Scale bar = 40 μ m. (F–G) The expression of Nrg1 and Crlf1 at RNA level in validation samples. (H) Immunohistochemistry staining of NRG1 and CRLF1 in Con and HTS tissues. Scale bar = 100 μ m. (I) Protein expression of NRG1 and CRLF1 detected by Western Blot in Con and HTS samples. (J–K) The relative quantification result of NRG1 and CRLF1 expression detected by Western Blot. * represents $p < 0.05$, ** represents $p < 0.01$. (For interpretation of the references to colour in this figure legend, the reader is referred to the web version of this article.)

compared to normal tissues (Fig. 5I-K).

4. Discussion

HTS is a common abnormal healing phenomenon that occurs during the repair of skin injuries, which can be caused by burns, trauma, acne, and post-surgery [17]. Despite various treatment options, such as laser therapy, surgery and cryotherapy, there is no consensus on the most effective and side-effect-free treatment for improving HTS. Recent studies have indicated that immune-related profiles may serve a vital function in the development of HTS [18]. In this study, we used RNA-seq analysis and WGCNA to provide the first evidence that CRLF1 and NRG1 could act as potential immune related signatures of HTS.

To gain a deeper understanding of the molecular pathways implicated in HTS, we performed RNA-seq analysis, which revealed a total of 940 DEGs between HTS and Con. Among these DEGs, 378 were up-regulated and 562 were downregulated. Further analysis using KEGG enrichment analysis suggested that DEGs were predominantly enriched in fibrosis related pathways, including focal adhesion, Wnt signaling pathway and excessive extracellular matrix (ECM)-receptor interaction. Focal adhesion is known to play a crucial role in transducing various signals and acting as a mechanical linkage to the ECM [19,20]. Additionally, ECM-receptor interactions are associated with abnormal scar formation.

WGCNA is a method to discover the complicated correlations between genes and phenotypes by constructing co-expression modules using gene expression profiles [21]. In this study, we employed WGCNA to find functional key module of HTS. KEGG and GO enrichment analysis indicated that genes in salmon module were related to 'Wnt signaling pathway', 'TNF signaling pathway' and immune related pathway including 'Th17 cell differentiation', 'Antigen processing and presentation' and 'B cell receptor signaling pathway'. The Wnt/ β -catenin signaling pathway differs significantly during the transition of scarring from the proliferative phase to the tissue remodel phase, and modulation of the Wnt signaling pathway may promote improvement in HTS in mouse trauma models [22]. Furthermore, activation of Wnt/ β -catenin pathway inhibited TGF- β 1-mediated renal fibrosis [23]. The tumour necrosis factor receptor-associated death domain protein (TRADD) has been reported to regulate proliferation and apoptosis of hypertrophic scar fibroblasts and to regulate type I collagen secretion through TNF- α -mediated signaling pathways [24]. Our study shows that the key genes including SP9, TBX2, HOXB6, MSX2 and KRT19 may highlights the potential function in salmon module and provides valuable insights into the molecular pathways associated with HTS.

Inflammatory cells are responsible for detecting damage associated molecular patterns (DAMPs) when injury and wound occurs [25]. Dysregulation of immune cells can lead to the abnormal scar and alter the outcome of wound healing. Th17 cells are a subpopulation of T lymphocytes, and their key cytokine IL-17 is markedly elevated in hypertrophic scar. Injection of recombinant IL-17 into the wound during the inflammatory phase can trigger an augmentation in fibrosis and exacerbate the existing inflammation [26]. It has been shown that TNF- α secreted by M1 macrophages is an important factor in scar formation [27]. Specifically, the effect of deposition of collagen could be alleviated by blocking PI3K-Akt signaling pathway in mast cells [28]. To investigate the role of immune cells and inflammatory factors in HTS, we utilized the ImmuPort database to explore key genes associated with immune response. Through this analysis, we identified eight immune related genes (IFI30, NR2F2, NRG1, ESM1, NFATC2, CRLF1, COLEC12 and IL6) by crossing CGs and 1793 immune-related genes in the ImmuPort database. Further analysis of the GSE136906 dataset confirmed the differential expression differences of CRLF1 and NRG1. To validate these findings, we performed qRT-PCR, immunohistochemistry staining, and Western blotting to measure the expression of CRLF1 and NRG1 in HTS and Con samples. We also discovered that activated mast cell had positive correlation with CRLF1 expression. Meanwhile, CD8 T cells was

positively correlated with NRG1.

Although immunotherapy is a potential therapeutic strategy for treating scar, the immune-related markers for HTS are incredibly scarce [29,30]. We identified CRLF1 and NRG1 as potential HTS biomarkers for the first time. Concerning the two characteristic genes screened by WGCNA and ImmuPort, we performed further investigation. CRLF1, a member of cytokines receptors, is involved in immune function, inflammation, haematopoiesis, cell growth and differentiation [31]. Previous studies have shown that CRLF1 promotes proliferation and metastasis of papillary thyroid carcinoma by activating ERK pathway in thyroid carcinoma cells [32]. In addition, overexpression of CRLF1 aggravated cardiac fibrosis by the activation of ERK1/2 signaling pathway [33]. Therefore, we speculated that CRLF1 might mediate the proliferation and migration of fibroblasts to participate in the construction of HTS. Previous studies have reported that NRG1 may contribute to keloid margin migration through ErbB2-mediated signaling [34]. Of note, NRG-1 β /ErbB-dependent activation of Src/Focal adhesion kinase could modulate cell motility and focal adhesion complex formation in Schwann cells [35]. Moreover, NRG1 has been shown to be a potent inducer of cardiomyocyte proliferation after cardiac impairment [36–38]. The above evidence demonstrated the value of NRG1 as a novel biomarker in fibrosis related diseases. We hypothesize that NRG1 may play a role in HTS formation by regulating the immune microenvironment, although the exact mechanism still requires further investigation.

Although our study yielded some valuable insights into the relationship between immune related genes and HTS, several limitations exist. An important limitation is the small sample size that consequently limited the effect size and statistical power of our results, thereby highlighting the need for further follow-up validation studies on a larger cohort. Additionally, the clinical information available for these samples was limited, which may have affected the interpretation of our results. Lastly, we mainly focus on the immune-related genes in this study and the key genes such as SP9 and KRT19 in the module of WGCNA appear to be significant in HTS and further exploration is warranted to better understand the roles of these genes. The precise mechanistic role of CRLF1 and NRG1 in the development of HTS remains unclear. In-depth in vivo experiments are needed to validate these findings and provide a better understanding of their mechanisms.

5. Conclusion

In conclusion, we utilized WGCNA approach to identify CRLF1 and NRG1 as immune-related characteristic genes associated with HTS. We conducted validation experiments using qRT-PCR, immunohistochemistry staining and Western Blot analysis. Overall, our findings contribute to the understanding of the molecular mechanism underlying HTS and provide valuable insights into the immunotherapy approach for HTS treatment.

Supplementary data to this article can be found online at <https://doi.org/10.1016/j.ygeno.2024.110797>.

Funding

None.

Ethics approval and Consent to participate

This study was approved by the Medical and Ethics Committees of the Fourth Medical Center of Chinese PLA General Hospital (2023KY140-KS001), and each patient signed an informed consent before enrolling in this study.

Consent for publication

All authors agree to publish.

CRedit authorship contribution statement

Boya Yu: Data curation, Writing – original draft. **Yalei Cao:** Conceptualization, Formal analysis. **Shiyi Li:** Investigation, Visualization. **Ruiqi Bai:** Software. **Guiwen Zhou:** Conceptualization, Investigation. **Qiang Fu:** Software, Validation. **Liming Liang:** Resources, Validation. **Weijie Gu:** Supervision, Visualization. **Lixia Zhang:** Project administration, Supervision. **Minliang Chen:** Conceptualization, Supervision, Writing – review & editing.

Declaration of competing interest

The authors have no competing interests to disclose.

Data availability

The transcriptome sequencing raw reads generated during this study are freely available at SRA (<https://www.ncbi.nlm.nih.gov/sra/>) under accession number PRJNA1026108. Publicly available datasets were analyzed in this study. This data can be found here: <https://www.ncbi.nlm.nih.gov/geo/>; GSE136906.

Acknowledgments

None.

References

- R. Ogawa, The Most current algorithms for the treatment and prevention of hypertrophic scars and keloids: a 2020 update of the algorithms published 10 years ago, *Plast Reconstr Surg* 149 (1) (2022) 79e–94e.
- C.C. Finnerty, M.G. Jeschke, L.K. Branski, J.P. Barret, P. Dziejewski, D.N. Herndon, Hypertrophic scarring: the greatest unmet challenge after burn injury, *Lancet* 388 (10052) (2016) 1427–1436.
- S. Amjadi, S. Moradi, P. Mohammadi, The emerging therapeutic targets for scar management: genetic and epigenetic landscapes, *Skin Pharmacol Physiol* 35 (5) (2022) 247–265.
- R. Leszczynski, C.A. da Silva, A.C.P.N. Pinto, U. Kuczynski, E.M. da Silva, Laser therapy for treating hypertrophic and keloid scars, *Cochrane Database Syst Rev* 9 (9) (2022) CD011642.
- T. Zhang, X.-F. Wang, Z.-C. Wang, D. Lou, Q.-Q. Fang, Y.-Y. Hu, W.-Y. Zhao, L.-Y. Zhang, L.-H. Wu, W.-Q. Tan, Current potential therapeutic strategies targeting the TGF- β /Smad signaling pathway to attenuate keloid and hypertrophic scar formation, *Biomed Pharmacother* 129 (2020) 110287.
- Y. Li, J. Zhang, J. Shi, K. Liu, X. Wang, Y. Jia, T. He, K. Shen, Y. Wang, J. Liu, W. Zhang, H. Wang, Z. Zheng, D. Hu, Exosomes derived from human adipose mesenchymal stem cells attenuate hypertrophic scar fibrosis by miR-192-5p/IL-17RA/Smad axis, *Stem Cell Res Ther* 12 (1) (2021) 221.
- C. Choi, I. Mukovozov, A. Jazdarehee, R. Rai, M. Sachdeva, M. Shunmugam, K. Zaslavsky, S. Byun, B. Barankin, Management of hypertrophic scars in adults: a systematic review and meta-analysis, *Australas J Dermatol* 63 (2) (2022) 172–189.
- J. Song, X. Li, J. Li, Emerging evidence for the roles of peptide in hypertrophic scar, *Life Sci* 241 (2020) 117174.
- Z.-C. Wang, W.-Y. Zhao, Y. Cao, Y.-Q. Liu, Q. Sun, P. Shi, J.-Q. Cai, X.Z. Shen, W.-Q. Tan, The roles of inflammation in keloid and hypertrophic scars, *Front Immunol* 11 (2020) 603187.
- M. Hesketh, K.B. Sahin, Z.E. West, R.Z. Murray, Macrophage phenotypes regulate scar formation and chronic wound healing, *Int J Mol Sci* 18 (7) (2017).
- A.P. Trace, C.W. Enos, A. Mantel, V.M. Harvey, Keloids and hypertrophic scars: a Spectrum of clinical challenges, *Am J Clin Dermatol* 17 (3) (2016) 201–223.
- D.E.A. Komi, K. Khomtchouk, P.L. Santa Maria, A review of the contribution of mast cells in wound healing: involved molecular and cellular mechanisms, *Clin Rev Allergy Immunol* 58 (3) (2020) 298–312.
- H. Cai, X. Liu, D. Liu, B. Liu, GEO data mining identifies potential immune-related genes in hypertrophic scar and verities in a rabbit model, *Heliyon* 9 (7) (2023) e17266.
- The Gene Ontology resource: Enriching a GOLD mine, *Nucleic Acids Res* 49 (D1) (2021) D325–D334.
- M. Kanehisa, M. Furumichi, Y. Sato, M. Ishiguro-Watanabe, M. Tanabe, KEGG: integrating viruses and cellular organisms, *Nucleic Acids Res* 49 (D1) (2021) D545–D551.
- A.M. Newman, C.L. Liu, M.R. Green, A.J. Gentles, W. Feng, Y. Xu, C.D. Hoang, M. Diehn, A.A. Alizadeh, Robust enumeration of cell subsets from tissue expression profiles, *Nat Methods* 12 (5) (2015) 453–457.
- J. Qi, Y. Liu, K. Hu, Y. Zhang, Y. Wu, X. Zhang, MicroRNA-26a inhibits hyperplastic scar formation by targeting Smad2, *Exp Ther Med* 15 (5) (2018) 4332–4338.
- B. Song, W. Liu, Y. Zhu, Y. Peng, Z. Cui, B. Gao, L. Chen, Z. Yu, B. Song, Deciphering the contributions of cuproptosis in the development of hypertrophic scar using single-cell analysis and machine learning techniques, *Front Immunol* 14 (2023) 1207522.
- A. Elosegui-Artola, X. Trepap, P. Roca-Cusachs, Control of Mechanotransduction by molecular clutch dynamics, *Trends Cell Biol* 28 (5) (2018) 356–367.
- H. Ngu, Y. Feng, L. Lu, S.J. Oswald, G.D. Longmore, F.C.P. Yin, Effect of focal adhesion proteins on endothelial cell adhesion, motility and orientation response to cyclic strain, *Ann Biomed Eng* 38 (1) (2010) 208–222.
- P. Langfelder, S. Horvath, WGCNA: an R package for weighted correlation network analysis, *BMC Bioinform* 9 (2008) 559.
- J. Zhu, M. Sun, Y. Wang, H. Bi, C. Xue, Gene expression profile analysis on different stages of hypertrophic scarring in a rabbit ear model, *Exp Ther Med* 20 (2) (2020) 1505–1513.
- C. Ho, P.-H. Lee, Y.-C. Hsu, F.-S. Wang, Y.-T. Huang, C.-L. Lin, Sustained Wnt/ β -catenin signaling rescues high glucose induction of transforming growth factor- β 1-mediated renal fibrosis, *Am J Med Sci* 344 (5) (2012) 374–382.
- Y. Yuan, G. Peng, X. Kang, Y. Liu, J. Dai, H. Wu, Effects of lentiviral vector-mediated TRADD expression on the inhibition of hypertrophic scar formation, *Exp Biol Med* (Maywood) 239 (12) (2014) 1557–1566.
- D. Tang, R. Kang, C.B. Coyne, H.J. Zeh, M.T. Lotze, PAMPs and DAMPs: signal Os that spur autophagy and immunity, *Immunol Rev* 249 (1) (2012) 158–175.
- J. Zhang, Q. Qiao, M. Liu, T. He, J. Shi, X. Bai, Y. Zhang, Y. Li, W. Cai, S. Han, H. Guan, D. Hu, IL-17 promotes scar formation by inducing macrophage infiltration, *Am J Pathol* 188 (7) (2018) 1693–1702.
- L. Chen, J. Wang, S. Li, Z. Yu, B. Liu, B. Song, Y. Su, The clinical dynamic changes of macrophage phenotype and function in different stages of human wound healing and hypertrophic scar formation, *Int Wound J* 16 (2) (2019) 360–369.
- Q. Zhang, A.P. Kelly, L. Wang, S.W. French, X. Tang, H.S. Duong, D.V. Messadi, A. D. Le, Green tea extract and (–)-epigallocatechin-3-gallate inhibit mast cell-stimulated type I collagen expression in keloid fibroblasts via blocking PI-3K/Akt signaling pathways, *J Invest Dermatol* 126 (12) (2006) 2607–2613.
- R. Ogawa, Keloid and hypertrophic scars are the result of chronic inflammation in the reticular dermis, *Int J Mol Sci* 18 (3) (2017).
- R. Ogawa, S. Akaishi, S. Kuribayashi, T. Miyashita, Keloids and hypertrophic scars can now be cured completely: recent Progress in our understanding of the pathogenesis of keloids and hypertrophic scars and the Most promising current therapeutic strategy, *J Nippon Med Sch* 83 (2) (2016) 46–53.
- L. Crisponi, I. Buers, F. Rutsch, CRLF1 and CLCF1 in development, health and disease, *Int J Mol Sci* 23 (2) (2022).
- S.-T. Yu, B.-H. Sun, J.-N. Ge, J.-L. Shi, M.-S. Zhu, Z.-G. Wei, T.-T. Li, Z.-C. Zhang, W.-S. Chen, S.-T. Lei, CRLF1-MYH9 interaction regulates proliferation and metastasis of papillary thyroid carcinoma through the ERK/ETV4 Axis, *Front Endocrinol (Lausanne)* 11 (2020) 535.
- S. Luo, Z. Yang, R. Chen, D. You, F. Teng, Y. Yuan, W. Liu, J. Li, H. Zhang, Cytokine receptor-like factor 1 (CRLF1) promotes cardiac fibrosis via ERK1/2 signaling pathway, *J Zhejiang Univ Sci B* 24 (8) (2023) 682–697.
- N. Jumper, T. Hodgkinson, R. Paus, A. Bayat, A role for Neuregulin-1 in promoting keloid fibroblast migration via ErbB2-mediated signaling, *Acta Derm Venereol* 97 (6) (2017) 675–684.
- S. Wakatsuki, T. Araki, A. Sehara-Fujisawa, Neuregulin-1/glia growth factor stimulates Schwann cell migration by inducing α 5 β 1 integrin-ErbB2-focal adhesion kinase complex formation, *Genes Cells* 19 (1) (2014) 66–77.
- G. D’Uva, A. Aharonov, M. Lauriola, D. Kain, Y. Yahalom-Ronen, S. Carvalho, K. Weisinger, E. Bassat, D. Rajchman, O. Yifa, M. Lysenko, T. Konfino, J. Hegesh, O. Brenner, M. Neeman, Y. Yarden, J. Leor, R. Sarig, R.P. Harvey, E. Tzahor, ERBB2 triggers mammalian heart regeneration by promoting cardiomyocyte dedifferentiation and proliferation, *Nat Cell Biol* 17 (5) (2015) 627–638.
- M. Gemberling, R. Karra, A.L. Dickson, K.D. Poss, Nrg1 is an injury-induced cardiomyocyte mitogen for the endogenous heart regeneration program in zebrafish, *Elife* 4 (2015).
- D.E.M. de Bakker, M. Bouwman, E. Dronkers, F.C. Simões, P.R. Riley, M.-J. Goumans, A.M. Smits, J. Bakkers, Prrx1b restricts fibrosis and promotes Nrg1-dependent cardiomyocyte proliferation during zebrafish heart regeneration, *Development* 148 (19) (2021).